Disturbance Observer-Based Quadrotor Attitude Tracking Control for Aggressive Maneuvers

Alberto Castillo[a,*], Ricardo Sanz[a], Pedro Garcia[a], Wei Qiu[b], Hongda Wang[b], Chao Xu[b]

[a] *Instituto de Automática e Informática Industrial, Universitat Politècnica de València, 46020 Valencia, Spain.*
[b] *Department of Control Science and Engineering, Zhejiang University, Hangzhou, China.*

Abstract

In this paper, a disturbance observer-based quadrotor attitude controller for aggressive maneuvering is presented. The controller is made up of the cascade connection between two control-loops: an outer quaternion-based attitude control-loop and an inner disturbance observer-based angular velocity tracking control-loop. The disturbance observer is designed to estimate and compensate for the Coriolis term and the external disturbances. It is shown that, for fast maneuvers, the disturbance observer needs to take into account the motor dynamics. This allows increasing notably the observer bandwidth, leading to significant improvements in the disturbance rejection capabilities. The stability of the resulting closed-loop is analyzed. Also, different simulations and flight tests are carried out to validate the main results, showing an outstanding tracking performance when aggressive attitude maneuvers are being executed, even in the presence of strong disturbances such as suspended payloads.

Keywords: Quadrotor, attitude control, quaternion, disturbance observer, mismatched disturbance, motor dynamics.

1. Introduction

Over the last years, the practical interest in quadrotor Unmanned Aerial Vehicles (UAVs) has increased notably. Their potential applications along with the advances in computer and sensor technologies, and their associated cost reductions, have hugely promoted the development of this kind of UAVs. This fact impulses to the research community to the study of new control strategies as any improvement in the quadrotor controller may lead to more robust and precise flight performance.

The first reports of a successful controlled quadrotor hover flight were published during 2002-2004 by different research groups (Altug et al., 2002; Bouabdallah et al., 2004; Castillo et al., 2003; Hoffmann et al., 2004). Since then, the number of studies about quadrotors has spiked notably and a wide number of studies about quadrotor control (Bouabdallah and Siegwart, 2007; Raffo et al., 2010; Guerrero-Castellanos et al., 2011; Tayebi, 2008; Tayebi and McGilvray, 2006; Lee, 2012; Lee et al., 2013), or quadrotor modelling/identification (Hoffmann et al., 2007; Erginer and Altug, 2007; Pounds et al., 2010; Chovancová et al., 2014; Derafa et al., 2006), can be found.

Although it is widely known that: i) the quadrotor's mathematical model is subject to topological constraints coming from the Special Orthogonal group, $SO(3)$, (Bhat and Bernstein, 2000; Mayhew et al., 2011; Schlanbusch et al., 2012); ii) the system performance is affected by the Coriolis effect (Pounds et al., 2010; Chovancová et al., 2014); iii) the motor's subsystem contains a non-negligible transient response (Madani and Benallegue, 2006; Derafa et al., 2006); and iv) the quadrotor model is quite sensitive to external disturbances (Liu et al., 2017); most of the proposed controllers are designed by neglecting some of these issues. In fact, the following assumptions are usually made: small angles, knowledge of the inertia matrix (in order to feed-forward the Coriolis term), fast motor dynamics and absence of external disturbances (Castillo et al., 2003; Hoffmann et al., 2004; Altug et al., 2002; Bouabdallah and Siegwart, 2007; Guerrero-Castellanos et al., 2011; Tayebi, 2008; Lee, 2012); which simplify the control design.

However, the recent heavy application demands in quadrotors let authors rethink about the consideration of those assumptions. In fact, small angles, fast motor dynamics and absence of external disturbances does not hold in many applications. For example, when the quadrotor operates in a windy environment, or when aggressive attitude maneuvering is required in large-size quadrotors. For these reasons, an actual research area in quadrotor control is focused on the design of controllers avoiding these restrictions. A quite common approach to this purpose is to develop controllers that make use of quaternion algebra (Tayebi, 2008; Fresk and Nikolakopoulos, 2013; Mazinan et al., 2015) and Disturbance Observer-Based (DOB) techniques (Chen and Huang, 2009; Liu and Wang, 2015;

*Corresponding author
Email address: alcasfra@gmail.com (Alberto Castillo)

Wang et al., 2015; Zhang et al., 2011; Zhang and Wang, 2015), which are able to attenuate external disturbances and model uncertainties. In fact, experiments have been reported where DOB controllers improve performance noticeably (Sanz et al., 2016; Wang and Su, 2015; Xiao and Yin, 2017). However, previous works still consider fast motors dynamics in the disturbance observer design, an assumption that is not valid when fast attitude maneuvers are being executed.

The main purpose of this work is to develop a novel quaternion-based DOB controller for quadrotors that is capable to carry out precise and aggressive attitude maneuvers in the presence of high disturbances. The proposed DOB controller estimates and compensates for the external disturbances and the Coriolis term. Furthermore, the motor dynamics are not neglected when designing the disturbance observer. Instead, it is considered that the motors dynamics are described by a first-order model (Michael et al., 2010). This fact constitutes the major departure from previous DOB quadrotor controllers and it also introduces difficulties in the controller design/analysis because the so-called disturbance matched condition (Chen et al., 2016; Castillo et al., 2018) does no longer hold, i.e. the external disturbances and the Coriolis term act in a different channel than the control action. Nonetheless, it will be shown that considering the motors dynamics allows increasing notably the observer bandwidth, leading to important improvements in the controller performance.

The tuning of the resulting controller turns out to be very intuitive and its implementation is relatively simple. Extensive experiments are performed on a large-size quadrotor prototype to illustrate the feasibility of this approach. The results show an outstanding performance, being able to track fast angular references (even carrying a suspended load) and perform precise 720 deg flips in 0.5 sec.

The rest of the paper is structured as follows. In Section 1.1 the main notation is introduced. In Section 2, the quadrotor mathematical model is presented and reformulated conveniently. The proposed controller is developed in Section 3 whereas its stability is analyzed in Section 4. Simulations and tuning guidelines are discussed in Section 5 and the experimental results are reported in Section 6. Finally, in Section 7, some conclusions are given.

1.1. Notation and preliminaries

Vectors are represented by lower case bold symbols and matrices by upper case bold symbols. The operator $\|\cdot\|$ denotes the standard Euclidean norm for vectors or the corresponding induced norm for matrices. For any vector $\boldsymbol{x} \in \mathbb{R}^3$, the skew-symmetric operator is defined by

$$\boldsymbol{S}(\boldsymbol{x}) \triangleq \begin{bmatrix} 0 & -x_3 & x_2 \\ x_3 & 0 & -x_1 \\ -x_2 & x_1 & 0 \end{bmatrix}.$$

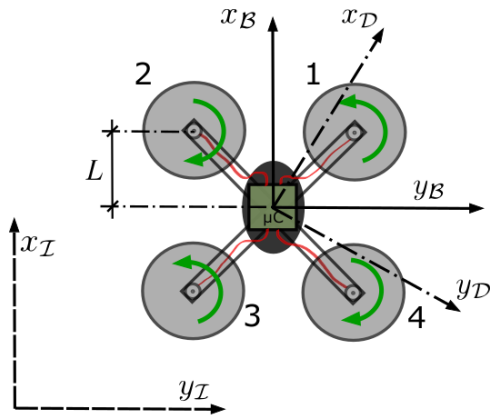

Figure 1: Inertial, body-fixed and desired reference frames. The goal in attitude control is that $\mathcal{B} \to \mathcal{D}$.

The inertial, body-fixed and desired attitude reference frames are denoted by $\mathcal{I}$, $\mathcal{B}$ and $\mathcal{D}$, respectively (see Fig. 1). A quaternion is denoted by $q \triangleq [q_0,\ \boldsymbol{q}]^T \in \mathbb{R}^4$, where $q_0 \in \mathbb{R}$ is the real part and $\boldsymbol{q} \in \mathbb{R}^3$ the vector part. The Hamilton quaternion product is represented by $\otimes$ while $(\cdot)^*$ is the quaternion conjugation operator (Kuipers et al., 1999). Finally, all quaternions appearing in this paper are considered to be unitary.

2. Quadrotor mathematical model

The attitude of a quadrotor is governed by the cascade connection of two differential equations: the kinematics and the dynamics. The kinematics relates the rate of change of an attitude measure from the body angular velocity, while the dynamics relates the rate of change of angular velocity from the external torques.

2.1. Quaternion-based kinematic model

The relative orientation between $\mathcal{B}$ and $\mathcal{I}$ is determined by a rotation $\theta_b \in \mathbb{R}$ along an unitary axis $\boldsymbol{u_b} \in \mathbb{R}^3$. This is parametrized by the quaternion

$$q_b \triangleq \begin{pmatrix} q_{b_0} \\ \boldsymbol{q_b} \end{pmatrix} = \begin{pmatrix} \cos(\theta_b/2) \\ \sin(\theta_b/2)\boldsymbol{u_b} \end{pmatrix} \tag{1}$$

whose associated rotation matrix, $\boldsymbol{R}$, is given by the Euler-Rodrigues formula (Shuster, 1993):

$$\boldsymbol{R}(q) = (q_0^2 - \boldsymbol{q}^T\boldsymbol{q})\boldsymbol{I_3} + 2\boldsymbol{q}\boldsymbol{q}^T + 2q_0\boldsymbol{S}(\boldsymbol{q}). \tag{2}$$

If $\mathcal{B}$ is rotating with respect to $\mathcal{I}$ with an angular velocity $\boldsymbol{\omega_b} \in \mathbb{R}^3$, then $q_b(t)$ satisfies that (see Theorem 3 of Jia (2013))

$$\begin{cases} \dot{q}_{b_0} = -\dfrac{1}{2}\boldsymbol{q_b}^T\boldsymbol{\omega_b}, \\ \dot{\boldsymbol{q}}_{\boldsymbol{b}} = \dfrac{1}{2}\left[q_{b_0}\boldsymbol{I_3} + \boldsymbol{S}(\boldsymbol{q_b})\right]\boldsymbol{\omega_b}, \end{cases} \tag{3}$$

which is considered as the quaternion-based quadrotor kinematic model.

2.2. Dynamic model

The quadrotor rotational dynamics can be described by the Newton's second law (Castillo et al., 2005):

$$\boldsymbol{J}\dot{\boldsymbol{\omega}}_{\boldsymbol{b}} = -\boldsymbol{S}(\boldsymbol{\omega}_{\boldsymbol{b}})\boldsymbol{J}\boldsymbol{\omega}_{\boldsymbol{b}} + \boldsymbol{\tau}_{\boldsymbol{u}} + \boldsymbol{\tau}_{\boldsymbol{\delta}}(\boldsymbol{t}), \tag{4}$$

where $-\boldsymbol{S}(\boldsymbol{\omega}_{\boldsymbol{b}})\boldsymbol{J}\boldsymbol{\omega}_{\boldsymbol{b}}$ is the torque produced by the Coriolis effect; $\boldsymbol{J} \in \mathbb{R}^{3\times 3}$ is the quadrotor inertia matrix, which is a symmetric positive definite matrix and assumed to be diagonal so that $\boldsymbol{J} \triangleq diag\{I_{xx}, I_{yy}, I_{zz}\}$; $\boldsymbol{\tau}_{\boldsymbol{u}}$ is the torque produced by the motors and $\boldsymbol{\tau}_{\boldsymbol{\delta}}(\boldsymbol{t})$ represents the torque produced by the external disturbances, which is assumed to satisfy the next property:

Assumption 1. *The external disturbance, $\boldsymbol{\tau}_{\boldsymbol{\delta}}(t)$, is continuous with first derivative bounded, i.e. $\|\dot{\boldsymbol{\tau}}_{\boldsymbol{\delta}}(t)\| \leq \beta_{\dot{\tau}_\delta}$ for some $\beta_{\dot{\tau}_\delta} \geq 0$.*

According to the configuration depicted in Fig. 1, the torques generated by the propellers can be modeled as

$$\begin{pmatrix}\tau_{u_1}\\ \tau_{u_2}\\ \tau_{u_3}\end{pmatrix} = \begin{bmatrix}-Lk_F & Lk_F & Lk_F & -Lk_F\\ Lk_F & Lk_F & -Lk_F & -Lk_F\\ k_M & -k_M & k_M & -k_M\end{bmatrix}\begin{pmatrix}(\Omega_1)^2\\ (\Omega_2)^2\\ (\Omega_3)^2\\ (\Omega_4)^2\end{pmatrix} \tag{5}$$

where L is the arm length, Ω_i denotes the rotational speed of the ith motor, and k_F, k_M are unknown constants. The motor speeds are usually expressed as a linear combination

$$\begin{pmatrix}(\Omega_1)^2\\ (\Omega_2)^2\\ (\Omega_3)^2\\ (\Omega_4)^2\end{pmatrix} = \begin{bmatrix}1 & -1 & 1 & 1\\ 1 & 1 & 1 & -1\\ 1 & 1 & -1 & 1\\ 1 & -1 & -1 & -1\end{bmatrix}\begin{pmatrix}\Omega_h\\ \delta\Omega_\phi\\ \delta\Omega_\theta\\ \delta\Omega_\psi\end{pmatrix} \tag{6}$$

where Ω_h is the total thrust and $\boldsymbol{\delta\Omega} \triangleq [\delta\Omega_\phi, \delta\Omega_\theta, \delta\Omega_\psi]^T$ are virtual control inputs generating torques in the x, y and z axis, respectively. The transformation matrix in (6) is non-singular and hence there is a one-to-one map between the virtual control inputs and the motors speed.

The variable $\boldsymbol{\delta\Omega}$ is often regarded in many works as the actual control input to the system. However, if high performance maneuvers are intended, the motor dynamics need to be taken into account. A simple model for the motors is given by (Michael et al., 2010):

$$\boldsymbol{\delta\dot{\Omega}} = -k_m\boldsymbol{\delta\Omega} + k_m\boldsymbol{u} \tag{7}$$

with $k_m > 0$ and $\boldsymbol{u} \triangleq [u_\phi, u_\theta, u_\psi]^T$, which is considered the manipulated variable in what follows.

Using (4)-(7), the attitude dynamics are given by

$$\begin{cases}\dot{\boldsymbol{\omega}}_{\boldsymbol{b}} = \boldsymbol{B}[\boldsymbol{\delta\Omega} + \boldsymbol{\sigma}(\boldsymbol{\omega}_{\boldsymbol{b}}, t)],\\ \boldsymbol{\delta\dot{\Omega}} = -k_m\boldsymbol{\delta\Omega} + k_m\boldsymbol{u},\end{cases} \tag{8}$$

where

$$\boldsymbol{\sigma}(\boldsymbol{\omega}_{\boldsymbol{b}}, t) \triangleq \boldsymbol{K_u}^{-1}\boldsymbol{\tau}_{\boldsymbol{\delta}}(t) - \boldsymbol{K_u}^{-1}\boldsymbol{S}(\boldsymbol{\omega}_{\boldsymbol{b}})\boldsymbol{J}\boldsymbol{\omega}_{\boldsymbol{b}},$$
$$\boldsymbol{K_u} \triangleq 4\,\mathrm{diag}[Lk_F,\ Lk_F,\ k_M]$$
$$\boldsymbol{B} \triangleq \mathrm{diag}[4Lk_F/I_{xx},\ 4Lk_F/I_{yy},\ 4k_M/I_{zz}].$$

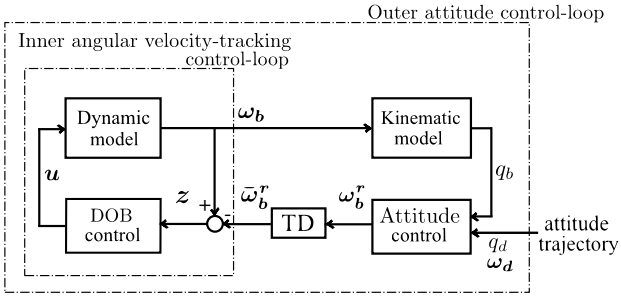

Figure 2: Block diagram of the control structure.

***Remark* 1.** *Note that $\boldsymbol{\sigma}(\boldsymbol{\omega}_{\boldsymbol{b}}, t)$ contains all the disturbances, that is, the external torques and the Coriolis term. This term will be estimated and compensated in real-time by the DOB control.*

3. Proposed control strategy

Almost all quadrotors are equipped with sensors that can be used to get measurements of q_b and $\boldsymbol{\omega_b}$. This permits to develop a cascade control strategy that it is formed by two sub-controllers: **i**). an outer attitude control-loop, which generates the angular velocity reference signal, $\boldsymbol{\omega}_{\boldsymbol{b}}^{\boldsymbol{r}}$; and **ii**). a DOB angular velocity tracking control-loop that generates the control action, $\boldsymbol{u}$, so that $\boldsymbol{\omega_b} \to \bar{\boldsymbol{\omega}}_{\boldsymbol{b}}^{\boldsymbol{r}}$.

The connection between both controllers is carried out through a Tracking Differentiator (TD). This is performed in order to introduce to the inner control-loop a smoothed angular velocity reference signal, $\bar{\boldsymbol{\omega}}_{\boldsymbol{b}}^{\boldsymbol{r}}$, with first derivative known. Figure 2 depicts a block diagram of the proposed controller.

3.1. Attitude controller

Let us consider that the desired attitude, $\mathcal{D}$, is generated by the same differential equation as the body kinematics (3):

Assumption 2. *The relative orientation between $\mathcal{D}$ and $\mathcal{I}$ is expressed by a trajectory, $q_d(t)$, satisfying*

$$\dot{q}_{d_0} = -\frac{1}{2}\boldsymbol{q_d}^T\boldsymbol{\omega_d}(t), \qquad \dot{\boldsymbol{q}}_{\boldsymbol{d}} = \frac{1}{2}\left[q_{d_0}\boldsymbol{I_3} + \boldsymbol{S}(\boldsymbol{q_d})\right]\boldsymbol{\omega_d}(t) \tag{9}$$

where the virtual angular velocity, $\boldsymbol{\omega_d}(t) \in \mathbb{R}^3$, satisfies that $\|\boldsymbol{\omega_d}(t)\| \leq \beta_{\omega_d}$, $\forall t \geq 0$, for some $\beta_{\omega_d} \geq 0$.

The attitude error, q_e, is defined as the relative orientation between $\mathcal{B}$ and $\mathcal{D}$, and it can be computed as

$$q_e \triangleq [q_{e_0}, \boldsymbol{q_e}]^T = (q_d)^* \otimes q_b. \tag{10}$$

The proposed kinematic control law is

$$\boldsymbol{\omega}_{\boldsymbol{b}}^{\boldsymbol{r}} = \boldsymbol{R}^T(q_e)\boldsymbol{\omega_d}(t) - k\boldsymbol{q_e} \tag{11}$$

where q_e is given by (10), $\boldsymbol{q_e}$ is the vector part of q_e, $\boldsymbol{R}^T(q_e)$ is given by (2) and $k \in \mathbb{R}$ is a positive constant for control tuning.

***Remark* 2.** *The control law* (11) *has a geometrical interpretation. As* $\boldsymbol{q_e}$ *has the direction of the rotation axis between* $\mathcal{D}$ *and* $\mathcal{B}$*, then* $k\boldsymbol{q_e}$ *is set in order to perform a rotation in such direction. The term* $\boldsymbol{R}^T(q_e)\boldsymbol{\omega_d}$ *is a feedforward term in order to compensate for the instant angular velocity of* $\mathcal{D}$*.*

***Remark* 3.** *In Castillo et al. (2016) it is proved that, if the transient responses of the TD and the angular velocity-tracking control-loop are neglected, i.e.* $\boldsymbol{\omega_b} \approx \boldsymbol{\omega_b^r}$*, then the control law* (11) *achieves exponential convergence of* $\boldsymbol{q_e}$ *to zero.*

***Remark* 4.** *For practical applications, in Section 5.2 it is explained how any Euler-angles-based user-commanded attitude trajectory can be transformed in order to satisfy Assumption 2.*

3.2. Tracking Differentiator

The following TD is employed:

$$\frac{\mathrm{d}}{\mathrm{d}t}\begin{pmatrix}\bar{\omega}^r_{b,i}\\ \dot{\bar{\omega}}^r_{b,i}\end{pmatrix} = \begin{bmatrix}0 & 1\\ -\omega_{td}^2 & -2\omega_{td}\end{bmatrix}\begin{pmatrix}\bar{\omega}^r_{b,i}\\ \dot{\bar{\omega}}^r_{b,i}\end{pmatrix} + \begin{bmatrix}0\\ \omega_{td}^2\end{bmatrix}\omega^r_{b,i}(t), \tag{12}$$

where $\omega^r_{b,i}$, $i \triangleq \{x, y, z\}$ represents each axis of the angular velocity reference signal generated by (11); $\bar{\omega}^r_{b,i}$ is the smoothed reference signal; and $\omega_{td} > 0$ is the TD bandwidth, which is a tuning parameter.

The TD has two main functions in the proposed controller. The first one is to produce a smooth angular velocity reference signal with first and second derivatives bounded. The second one is that it immediately provides the exact value of $\dot{\bar{\boldsymbol{\omega}}}^{\boldsymbol{r}}_{\boldsymbol{b}}$ which must be known for the dynamic controller as shown in next section.

3.3. Angular velocity-tracking controller

Let us consider the following assumption for the angular velocity-tracking control design.

Assumption 3. *The matrix* $\boldsymbol{B}$ *and the motor dynamics,* k_m*, are known.*

Assumption 3 does not constitute a major problem since those parameters can be easily identified in practice, even without the need of explicitly knowing the inertia matrix, $\boldsymbol{J}$, or k_F, k_M.

The proposed dynamic control law is

$$\boldsymbol{u} = \boldsymbol{B}^{-1}\left(-\boldsymbol{K}\boldsymbol{z} + \dot{\bar{\boldsymbol{\omega}}}^{\boldsymbol{r}}_{\boldsymbol{b}}\right) - \hat{\boldsymbol{\sigma}}, \tag{13}$$

where $\boldsymbol{z} \triangleq \boldsymbol{\omega_b} - \bar{\boldsymbol{\omega}}^{\boldsymbol{r}}_{\boldsymbol{b}}$ is the angular velocity-tracking error; $\boldsymbol{K} \succ 0$ is the feedback gain matrix, which is a controller tuning parameter; and $\hat{\boldsymbol{\sigma}}$ is an estimation of the lumped uncertainty, $\boldsymbol{\sigma}(\boldsymbol{\omega_b}, t)$, which is given by the following disturbance observer:

$$\dot{\hat{\boldsymbol{\Omega}}} = -k_m\hat{\boldsymbol{\Omega}} + k_m\boldsymbol{u} \tag{14}$$

$$\dot{\boldsymbol{\xi}} = -\boldsymbol{\Lambda}\boldsymbol{\xi} - \boldsymbol{\Lambda}^2\boldsymbol{B}^{-1}\boldsymbol{\omega_b} - \boldsymbol{\Lambda}\hat{\boldsymbol{\Omega}} \tag{15}$$

$$\hat{\boldsymbol{\sigma}} = \boldsymbol{\xi} + \boldsymbol{\Lambda}\boldsymbol{B}^{-1}\boldsymbol{\omega_b} \tag{16}$$

where $\boldsymbol{\Lambda} \triangleq \mathrm{diag}\,[\Lambda_{11}, \Lambda_{22}, \Lambda_{33}]^T$, $\Lambda_{ii} > 0$ is the observer bandwidth, which is also a tuning parameter.

***Remark* 5.** *The control law* (13) *has been designed considering the conventional assumption of fast motor dynamics, i.e.* $\boldsymbol{\delta\Omega} \approx \boldsymbol{u}$*. In this sense, equation* (13) *is designed to reject the effect of* $\boldsymbol{\sigma}(\boldsymbol{\omega_b}, t)$ *and to drive* $\boldsymbol{z} \to 0$ *with exponential decay-rate. However, note that the motor dynamics are taken into account when computing the observer in equation* (14)*. This is because, in practical applications, it is interesting to choose the observer bandwidth,* $\boldsymbol{\Lambda}$*, as large as possible in order to obtain fast estimations of the lumped disturbance. For aggressive maneuvers, the interesting values are higher than the the motors dynamics. As it will be shown latter, neglecting the motors dynamics in the disturbance observer design imposes a severe limitation on the achievable disturbance rejection performance.*

4. Closed-loop stability analysis

In this section the closed-loop system is studied. First the stability of the disturbance observer (14)-(16) is analyzed. Then, the stability of the angular velocity-tracking control-loop is studied and, finally it is shown that, if the angular velocity-tracking control-loop is stable, then the attitude error can be confined in a finite (small) region around $q_e = [1, 0, 0, 0]^T$.

4.1. Disturbance Observer stability

Let us define the observation error as

$$\tilde{\boldsymbol{\sigma}} \triangleq \boldsymbol{\sigma}(\boldsymbol{\omega_b}, t) - \hat{\boldsymbol{\sigma}}. \tag{17}$$

Then, the following result can be stated.

Proposition 1. *Assuming that the initial conditions satisfy* $\boldsymbol{\delta\Omega}(0) = \boldsymbol{\delta}\hat{\boldsymbol{\Omega}}(0)$*, then, the output of the observer* (14)-(16) *provides an estimation of the unknown dynamics such that the estimation error* (17) *satisfies*

$$\dot{\tilde{\boldsymbol{\sigma}}} = -\boldsymbol{\Lambda}\tilde{\boldsymbol{\sigma}} + \dot{\boldsymbol{\sigma}}(\boldsymbol{\omega_b}, t) \tag{18}$$

Proof. Differentiating (16) and using (8), (15) and (16), it follows that $\dot{\tilde{\boldsymbol{\sigma}}} = \boldsymbol{\Lambda}\tilde{\boldsymbol{\sigma}} + \boldsymbol{\Lambda}\left(\boldsymbol{\delta\Omega} - \boldsymbol{\delta}\hat{\boldsymbol{\Omega}}\right)$. Since the constant k_m is assumed to be known and $\boldsymbol{\delta}\hat{\boldsymbol{\Omega}}(0) = \boldsymbol{\delta\Omega}(0)$ then $\boldsymbol{\delta}\hat{\boldsymbol{\Omega}} \equiv \boldsymbol{\delta\Omega}$, refer to (7) and (14). The proposition follows by differentiating (17) and substituting $\dot{\tilde{\boldsymbol{\sigma}}} = -\dot{\tilde{\boldsymbol{\sigma}}} + \dot{\boldsymbol{\sigma}}(\boldsymbol{\omega_b}, t)$. □

4.2. Angular velocity-tracking closed-loop stability

Note that, as the motor dynamics are being considered, the quadrotor dynamic model (8) does not satisfy the so-called matched condition, i.e. the control action, $\boldsymbol{u}$, and the lumped disturbance, $\boldsymbol{\sigma}(\boldsymbol{\omega_b}, t)$, does not appear in the same channel. So, for analysis purposes, let us translate

the control action and the disturbance term into the same channel by rewriting (8) as

$$\begin{cases} \dot{\boldsymbol{z}} = \boldsymbol{B}\left[\boldsymbol{u} + \boldsymbol{\delta\tilde{\Omega}} + \boldsymbol{\sigma}(\boldsymbol{\omega_b}, t)\right] - \dot{\tilde{\boldsymbol{\omega}}}_{\boldsymbol{b}}^{\boldsymbol{r}} \\ \dot{\boldsymbol{\delta\tilde{\Omega}}} = -k_m \boldsymbol{\delta\tilde{\Omega}} - \dot{\boldsymbol{u}} \end{cases} \tag{19}$$

where $\boldsymbol{\delta\tilde{\Omega}} \triangleq \boldsymbol{\delta\Omega} - \boldsymbol{u}$.

Now, the expressions (13), (17)-(19) lead to the following closed-loop system:

$$\dot{\boldsymbol{x}} = \begin{bmatrix} -\boldsymbol{K} & \boldsymbol{B} & \boldsymbol{B} \\ 0 & -\boldsymbol{\Lambda} & 0 \\ 0 & 0 & -k_m I_3 \end{bmatrix} \boldsymbol{x} + \begin{bmatrix} 0 \\ \dot{\boldsymbol{\sigma}} \\ -\dot{\boldsymbol{u}} \end{bmatrix} \tag{20}$$

where $\boldsymbol{x} \triangleq [\boldsymbol{z}^T, \tilde{\boldsymbol{\sigma}}^T, \boldsymbol{\delta\tilde{\Omega}}^T]^T$.

Note that $\dot{\boldsymbol{u}}$ can be expressed in terms of $\boldsymbol{x}$. By adding and subtracting $\boldsymbol{\sigma}(\boldsymbol{\omega_b}, t)$ into (13), substituting (17) into the resulting expression, differentiating it, and then, incorporating (18) and (20), it is obtained that

$$\dot{\boldsymbol{u}} = \begin{bmatrix} \boldsymbol{B}^{-1}\boldsymbol{K}^2 & -\boldsymbol{B}^{-1}\boldsymbol{K}\boldsymbol{B} - \boldsymbol{\Lambda} & -\boldsymbol{B}^{-1}\boldsymbol{K}\boldsymbol{B} \end{bmatrix} \boldsymbol{x} + \boldsymbol{B}^{-1}\ddot{\boldsymbol{\omega}}_{\boldsymbol{b}}^{\boldsymbol{r}}. \tag{21}$$

Therefore, by (20)-(21), the closed-loop system results in

$$\dot{\boldsymbol{x}} = \boldsymbol{A}\boldsymbol{x} + d(t, \boldsymbol{x}) \tag{22}$$

with

$$\boldsymbol{A} \triangleq \begin{bmatrix} -\boldsymbol{K} & \boldsymbol{B} & \boldsymbol{B} \\ 0 & -\boldsymbol{\Lambda} & 0 \\ -\boldsymbol{B}^{-1}\boldsymbol{K}^2 & \boldsymbol{B}^{-1}\boldsymbol{K}\boldsymbol{B} + \boldsymbol{\Lambda} & \boldsymbol{B}^{-1}\boldsymbol{K}\boldsymbol{B} - k_m I_3 \end{bmatrix}$$

and $d(t, \boldsymbol{x}) \triangleq [0, \dot{\boldsymbol{\sigma}}, -\boldsymbol{B}^{-1}\ddot{\tilde{\boldsymbol{\omega}}}_{\boldsymbol{b}}^{\boldsymbol{r}}]^T$.

At this point, the next stability result can be stated

Theorem 1. *Consider that $\boldsymbol{A}$ is Hurwitz, that $\|\dot{\boldsymbol{\sigma}}\| \leq \beta_{\sigma_1}\|\boldsymbol{x}\| + \beta_{\sigma_2}$, $\|\ddot{\tilde{\boldsymbol{\omega}}}_{\boldsymbol{b}}^{\boldsymbol{r}}\| \leq \beta_{\ddot{\tilde{\omega}}_b^r}$ for all $\|\boldsymbol{x}\| \leq \beta_{\sigma_3}$, with $\beta_{\sigma_1}, \beta_{\sigma_2}, \beta_{\sigma_3}, \beta_{\ddot{\tilde{\omega}}_b^r} \geq 0$; and that*

$$\beta_{\sigma_1} < \frac{\underline{\lambda}(\boldsymbol{P}\boldsymbol{A} + \boldsymbol{A}^T\boldsymbol{P})}{2\|\boldsymbol{P}_2\|},$$

$$\beta_{\sigma_3} \geq \frac{2\|\boldsymbol{P}_3\boldsymbol{B}^{-1}\|\beta_{\ddot{\tilde{\omega}}_b^r} + 2\|\boldsymbol{P}_2\|\beta_{\sigma_2}}{\underline{\lambda}(\boldsymbol{P}\boldsymbol{A} + \boldsymbol{A}^T\boldsymbol{P}) - 2\|\boldsymbol{P}_2\|\beta_{\sigma_1}} \triangleq x^*,$$

where $\underline{\lambda}(\cdot) \triangleq min\{|\lambda_1(\cdot)|, |\lambda_2(\cdot)|, ...\}$, being $\lambda_i(\cdot)$ the eigenvalues of a given matrix; and $\boldsymbol{P} \triangleq [\boldsymbol{P}_1, \boldsymbol{P}_2, \boldsymbol{P}_3] \succ 0$ a solution to the Lyapunov equation $(\boldsymbol{P}\boldsymbol{A} + \boldsymbol{A}^T\boldsymbol{P}) \prec 0$.

Then, for any $\|\boldsymbol{x}(0)\| \leq x^*$, $\|\boldsymbol{x}(t)\| \leq x^*$ for all t.

Proof. See Appendix A □

Theorem 1 relies on the assumption of the existence of some constants $\beta_{\sigma_1}, \beta_{\sigma_2}, \beta_{\sigma_3}, \beta_{\ddot{\tilde{\omega}}_b^r}$, such that $\|\dot{\boldsymbol{\sigma}}\| \leq \beta_{\sigma_1}\|\boldsymbol{x}\| + \beta_{\sigma_2}$, $\forall\ \|\boldsymbol{x}\| \leq \beta_{\sigma_3}$ and $\|\ddot{\tilde{\boldsymbol{\omega}}}_{\boldsymbol{b}}^{\boldsymbol{r}}\| \leq \beta_{\ddot{\tilde{\omega}}_b^r}$. The next proposition establishes its existence.

Proposition 2. *Under Assumptions 1, 2, and if the angular velocity reference signal $\boldsymbol{\omega_b^r}$ generated by (11) is smoothed by the TD (12); then, there exists $\beta_{\sigma_1}, \beta_{\sigma_2}, \beta_{\sigma_3}, \beta_{\ddot{\tilde{\omega}}_b^r} \geq 0$ such that $\|\dot{\boldsymbol{\sigma}}\| \leq \beta_{\sigma_1}\|\boldsymbol{x}\| + \beta_{\sigma_2}$, $\forall\ \|\boldsymbol{x}\| \leq \beta_{\sigma_3}$ and $\|\ddot{\tilde{\boldsymbol{\omega}}}_{\boldsymbol{b}}^{\boldsymbol{r}}\| \leq \beta_{\ddot{\tilde{\omega}}_b^r}$.*

Proof. See Appendix B □

4.3. Attitude control-loop stability

The following theorem states that if the angular velocity-tracking control-loop is stable, then the attitude error, $\|\boldsymbol{q_e}\|$, is confined in a region around $q_e = [1, 0, 0, 0]^T$.

Theorem 2. *Consider that Assumption 2, and the conditions of Theorem 1, hold. Then, there exist constants, $\epsilon_z \triangleq \max\{\|\boldsymbol{z}(t)\|\}$, $\epsilon_\omega \triangleq \max\{\|\boldsymbol{\omega}_b^r(t) - \bar{\boldsymbol{\omega}}_{\boldsymbol{b}}^{\boldsymbol{r}}(t)\|\}$, such that, if $q_{e_0}(0) > \sqrt{1 - \left(\frac{\epsilon_z + \epsilon_\omega}{k}\right)^2}$ and $k > \epsilon_z + \epsilon_\omega$, then, for all t, the attitude error is bounded by*

$$q_{e_0}(t) \geq \sqrt{1 - \left(\frac{\epsilon_z + \epsilon_\omega}{k}\right)^2} > 0,$$
$$\|\boldsymbol{q_e}(t)\| \leq \frac{\epsilon_z + \epsilon_\omega}{k} < 1. \tag{23}$$

Proof. See Appendix C. □

Theorems 1-2 say that the closed-loop control system can be stabilized with an appropriate choice of the controller parameters. This result is normally known as practical stability (Hahn, 1967).

On the one hand, Proposition 2 establishes the existence of some constants $\beta_{\sigma_1}, \beta_{\sigma_2}, \beta_{\sigma_3}, \beta_{\ddot{\tilde{\omega}}_b^r} \geq 0$ such that the disturbance terms in (22) are bounded by $\|\dot{\boldsymbol{\sigma}}\| \leq \beta_{\sigma_1}\|\boldsymbol{x}\| + \beta_{\sigma_2}$, $\|\ddot{\tilde{\boldsymbol{\omega}}}_{\boldsymbol{b}}^{\boldsymbol{r}}\| \leq \beta_{\ddot{\tilde{\omega}}_b^r}$, for all $\|\boldsymbol{x}\| \leq \beta_{\sigma_3}$. Theorem 1 states that, by varying the controller parameters, $\boldsymbol{K}$, $\boldsymbol{\Lambda}$, the stability bounds, and the attractive region, for a given β_{σ_1}, β_{σ_3} can be increased or decreased. On the other hand, Theorem 2 states that, if the angular velocity-tracking control-loop is stable, then, the attitude error can be confined in a small region, whose size depends on the quotient between k and $\epsilon_z + \epsilon_\omega$, being ϵ_z, ϵ_ω, the upper bounds of the angular velocity tracking error and the error caused by the TD.

5. Controller Tuning Guidelines and Simulations

This section presents some tuning guidelines that are useful for controller gain setting. Also, a methodology to generate attitude trajectories satisfying Assumption 2 is proposed. Moreover, several simulation results are included in order to show the main features of the proposed control strategy.

5.1. Controller tuning

Kinematic and dynamic feedback gains: The gains $\boldsymbol{K}$ and k are parametrized by a single scalar, which is related with the characteristic time of the closed-loop.

Let us assume that there are no external disturbances, $\boldsymbol{\tau_\delta}(t) = 0$, that $\boldsymbol{u} \equiv \boldsymbol{\delta\Omega}$ and that the TD (12) accurately follows the input signal. Then, the linearized quadrotor model around $\boldsymbol{q_e} = 0$ and $\boldsymbol{w_b} = 0$ is given by

$$\ddot{\bar{\eta}} = b_\eta u_\eta - \ddot{\eta}^r, \qquad \eta \triangleq \{\phi, \theta, \psi\} \tag{24}$$

where $\bar{\eta} \triangleq \eta - \eta^r$, while η represents each of the Euler angles. By using small-angles approximation, $\boldsymbol{q_e}$ can be written as

$$\boldsymbol{q_e} \approx \left[\frac{\phi - \phi^r}{2}, \frac{\theta - \theta^r}{2}, \frac{\psi - \psi^r}{2}\right]^T, \tag{25}$$

and, by using (24)-(25), the control (13) with $\boldsymbol{K} = \text{diag}\{k_\phi, k_\theta, k_\psi\}$ can be approximately written as

$$u_\eta = \frac{1}{b_\eta}\left[-\frac{k k_\eta}{2}(\eta - \eta^r) - \left(\frac{k}{2} + k_\eta\right)(\dot{\eta} - \dot{\eta}^r) + \ddot{\eta}^r\right]$$

which, plugged into (24), yields the characteristic polynomial

$$s^2 + \left(\frac{k}{2} + k_\eta\right) s + \frac{k}{2} k_\eta = 0.$$

A simple tuning consists of selecting $k = 2\tau_\eta^{-1}$ and $k_\eta = \tau_\eta^{-1}$ where τ_η is the desired characteristic closed-loop time of the η-axis. Typical values for τ_η in quadrotor systems range between 0.15 s and 0.25 s for the roll and pitch axes, and between 0.2 s and 0.75 s for the yaw axis.

***Remark* 6.** *Note that if τ_η is reduced, then K and k are increased. This contributes to: i) reducing the attractive region of Theorem 1, ii) reducing ϵ_z in Theorem 2 and, iii) reducing the attractive region of Theorem 2.*

Disturbance observer and TD: The disturbance observer is tuned by following the typical approach in DOB controllers. By Proposition 1, the disturbance observation error can be seen a high-pass filter of the signal $\dot{\boldsymbol{\sigma}}(\cdot)$, whose cut-off frequency directly depends on $\boldsymbol{\Lambda}$. By increasing $\boldsymbol{\Lambda}$, disturbances of higher frequencies can be observed. Therefore, its bandwidth should be designed to filter out all the important frequencies contained in $\dot{\boldsymbol{\sigma}}(\cdot)$. These frequencies are related with the angular velocity/acceleration of the quadrotor's maneuvers, and, also, with the maximum frequency of $\dot{\boldsymbol{\tau}}_\delta(t)$. The most appropriate choice for this parameter may depend on each particular application. In this paper, it is experimentally found that, if aggressive maneuvers are going to be executed, then, the disturbance observer bandwidth should be between 50-100 Hz. Finally, the main purpose of the TD is to produce a smoothed angular velocity reference signal, $\bar{\boldsymbol{\omega}}_{\boldsymbol{b}}^{\boldsymbol{r}}$, with first derivative known. Hence, its bandwidth should be designed to follow all the frequencies contained in $\boldsymbol{\omega}_{\boldsymbol{b}}^{\boldsymbol{r}}$ in order to reduce, as much as possible, the error introduced by the TD in the control-loop, i.e. reducing the parameter ϵ_ω in Theorem 2. These frequencies are related with the angular velocity of the quadrotor's maneuvers. In this paper it is found that, if the TD bandwidth is between 100-200 Hz, then the errors introduced in the closed-loop by the TD can be almost ignored.

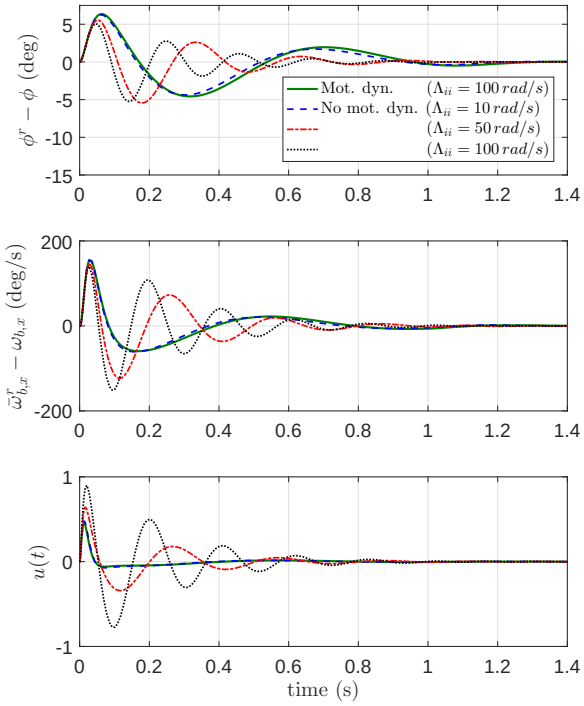

Figure 3: Effect of considering the motor dynamics in the disturbance observer design. The observer bandwidth can be increased up 100 rad/s without producing oscillations in the control action.

Mot. dyn.	**ISE**$\{\phi^r - \phi\}$	**TV**$\{u\}$
$\Lambda_{ii} = 100$ rad/s	7.5998	1.0801
No Mot. dyn.	**ISE**$\{\phi^r - \phi\}$	**TV**$\{u\}$
$\Lambda_{ii} = 10$ rad/s	6.7183	1.1502
$\Lambda_{ii} = 50$ rad/s	4.5564	2.7090
$\Lambda_{ii} = 100$ rad/s	3.2590	5.9214

Table 1: Integral Squared Error (ISE) and Total Variation (TV) of signals in Figure 3

5.2. Generation of Attitude Trajectories

Assumption 2 states that the desired attitude trajectory, $q_d(t)$, needs to be generated by the same differential equation as the body kinematics (11). Also, in order to compute the control law (11), the variable $\boldsymbol{\omega_d}(t)$ needs to be known. In this section it is shown how to generate a trajectory satisfying Assumption 2.

In most practical applications, it is easier for the pilot to introduce the attitude reference signal in terms of the Euler-angles. If a feasible trajectory

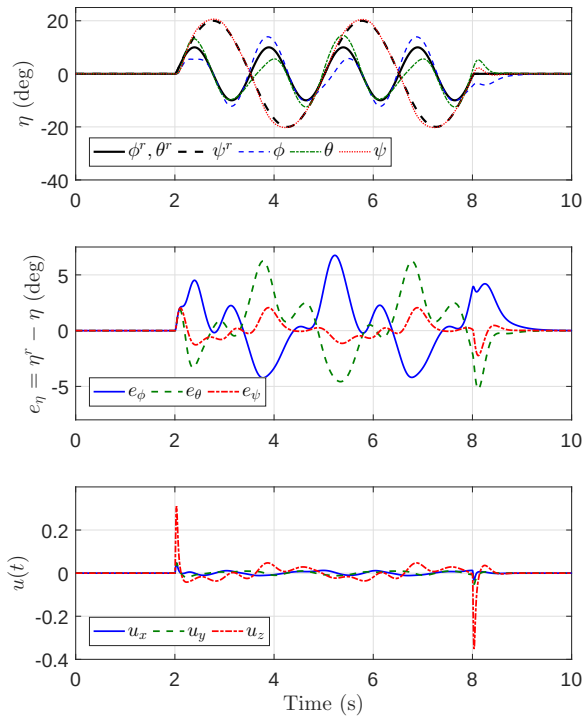

Figure 4: Sinusoidal reference tracking errors when the disturbance estimation is not feed-forward.

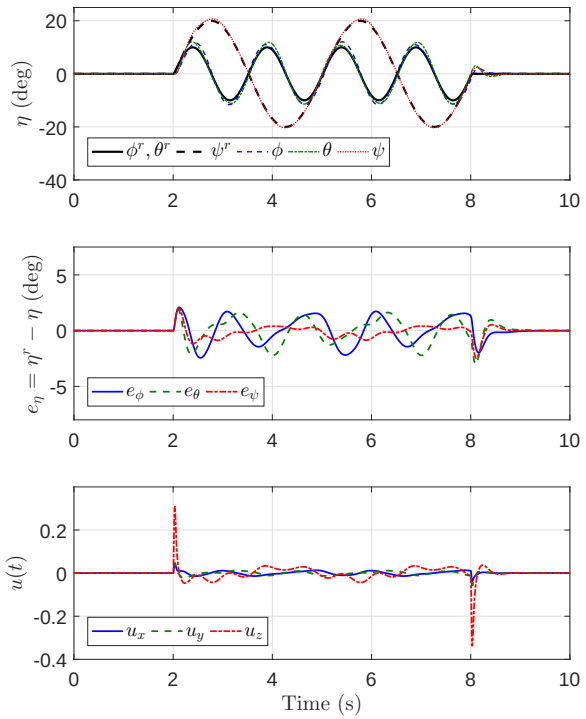

Figure 5: Sinusoidal reference tracking errors when the disturbance estimation is feed-forward.

	RMS$\{\phi, \theta, \psi\}$	**TV**$\{u\}$
With DOB	$\{0.96, 0.93, 0.42\}$ deg	0.3818
Without DOB	$\{2.31, 2.39, 0.66\}$ deg	0.3686

Table 2: Root Mean Square (RMS) and Total Variation (TV) of signals in Figs 4, 5

$\eta^r(t) \triangleq \{\phi^r(t), \theta^r(t), \psi^r(t)\} \in \mathcal{C}^1$ is given, then Assumption 2 is satisfied and $\boldsymbol{\omega_d}(t)$ is given by

$$\boldsymbol{\omega_d} = \begin{bmatrix} 1 & 0 & -\sin\theta^r \\ 0 & \cos\phi^r & \sin\phi^r \cos\theta^r \\ 0 & -\sin\phi^r & \cos\phi^r \cos\theta^r \end{bmatrix} \begin{pmatrix} \dot{\phi}^r \\ \dot{\theta}^r \\ \dot{\psi}^r \end{pmatrix} \tag{26}$$

If a feasible $\eta^r(t)$ is not given, let us assume that a generator reference signal $\eta^{rc}(t) \triangleq \{\phi^{rc}(t), \theta^{rc}(t), \psi^{rc}(t)\} \notin \mathcal{C}^1$ is available (in practice, this signal may come from a remote controller or any other source). Then $\eta^{rc}(t)$ is smoothed by using the same TD as the one in (12), providing a feasible $\eta^r(t) \in \mathcal{C}^1$ with first derivative known. That is:

$$\frac{\mathrm{d}}{\mathrm{d}t}\begin{pmatrix} \eta^r(t) \\ \dot{\eta}^r(t) \end{pmatrix} = \begin{bmatrix} 0 & 1 \\ -\omega_{td_r}^2 & -2\omega_{td_r} \end{bmatrix} \begin{pmatrix} \eta^r(t) \\ \dot{\eta}^r(t) \end{pmatrix} + \begin{bmatrix} 0 \\ \omega_{td_r}^2 \end{bmatrix} \eta^{rc}(t), \tag{27}$$

where ω_{td_r} is the reference-signal TD bandwidth, which should be chosen sufficiently large so that the smoothed reference-signal, $\eta^r(t)$, is able to accurately follow to $\eta^{rc}(t)$. Then, $\boldsymbol{\omega_d}$ is computed by (26).

***Remark* 7.** *It should be remarked that the Euler angles are only used for a more human-friendly interaction. The reference trajectories are converted to quaternion representation (Shuster, 1993), and then, the control law* (10)-(11) *is computed in terms of quaternions.*

5.3. Simulations

The only parameters that need to be identified in order to compute the control law (13) are $\boldsymbol{B}$ and k_m. A wide number of techniques have been developed for quadrotor parameter identification (Hoffmann et al., 2007; Chovancová et al., 2014; Derafa et al., 2006; Michael et al., 2010) that can be used to obtain $\boldsymbol{B}$ and k_m. In this case, a naive identification to match the quadrotor dynamic model (8) leads to $\boldsymbol{B} = \mathrm{diag}\{400, 400, 60\}$ and $k_m = 1/0.05\ s^{-1}$. All the simulations below are carried out using these values. Furthermore, the following parameters are selected for simulation purposes: $\boldsymbol{J} = \mathrm{diag}\{0.002, 0.002, 0.015\}\ kg \cdot m^2$, $k_F = 1.3$, $k_M = 0.25$, $L = 15$ cm; and they are not needed in the control law implementation. The feedback-gains have been chosen according to Section 5.1 with $\tau_\phi = \tau_\theta = \tau_\psi = 0.2$ sec. Finally, the disturbance observer bandwidth is set to $\Lambda_{ii} = 100\,\mathrm{rad/s}$, while the TD (12) bandwidth is set to $w_{td} = 200$ rad/s.

Three simulations are carried out in order to show three different features of the proposed controller, which are: **i**) The advantages of considering the motor dynamics in the disturbance observer design; **ii**) The ability of controller when attenuating the Coriolis effect and its performance in trajectory tracking; and **iii**) The ability of controller when attenuating unknown external disturbances.

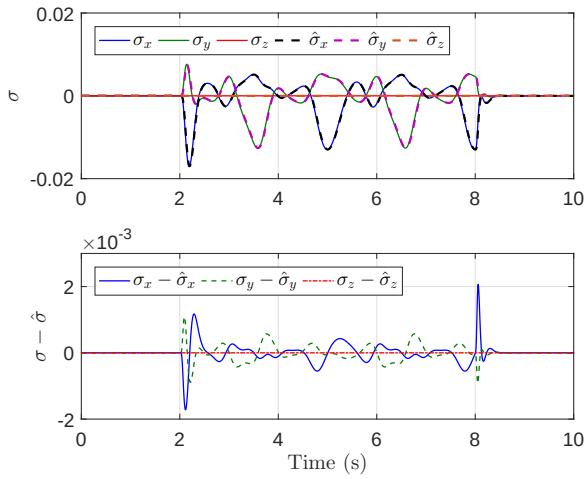

Figure 6: Unknown elements, i.e. Coriolis effect, and its estimation by the DOB.

	RMS$\{\phi\}$	**TV**$\{u\}$
With DOB	0.3846 deg	0.4393
Without DOB	2.4716 deg	0.1867

Table 3: Root Mean Square (RMS) and Total Variation (TV) of signals in Figure 7

The first simulation results are shown in Fig. 3 and Table 1. A step trajectory $\eta_1^{rc}(t) = \{10, 0, 0\} \notin \mathcal{C}^1$, $\forall t > 0$ is commanded. According to Section 5.2, since $\eta_1^{rc}(t)$ does not satisfy Assumption 2, it is smoothed by (27) with $\omega_{td_r} = 50$ rad/s. The comparison shows the control performance when the observer is computed by (14)-(16) (green line) and when it is computed neglecting the motors dynamics, i.e. setting $k_m \approx \infty$ in (14), (red, blue and black lines). The results show that neglecting the motor dynamics leads to oscillations in the control action as the observer bandwidth is increased. This reveals that, for fixed k and $\boldsymbol{K}$, higher values in the disturbance observer bandwidth can be chosen if the rotors dynamics are taken into account, enhancing the disturbance rejection capabilities.

For the second simulation, the following trajectory is commanded:

$$\eta_2^{rc}(t) = \{10\sin(2\pi/1.5t), 10\sin(2\pi/1.5t), 20\sin(2\pi/3t)\},$$

for all $t \in [2, 8]$. Note that, as the trajectory is performed simultaneously in the three axis, the Coriolis term is not negligible, but the proposed disturbance observer (14)-(16) should estimate and compensate for it. Simulation results are shown in Figs. 4-6 and Table 2. Figure 4 depicts the simulation results when the disturbance estimations are not feed-forward in (13), i.e. $\hat{\sigma}$ is set to zero. Figure 5 depicts the results when the disturbance estimations are feed-forward and Figure 6 represents the observation and observation error of the Coriolis term. It can be seen how the trajectory tracking is enhanced due to the disturbance observer, which is capable to estimate the Coriolis term.

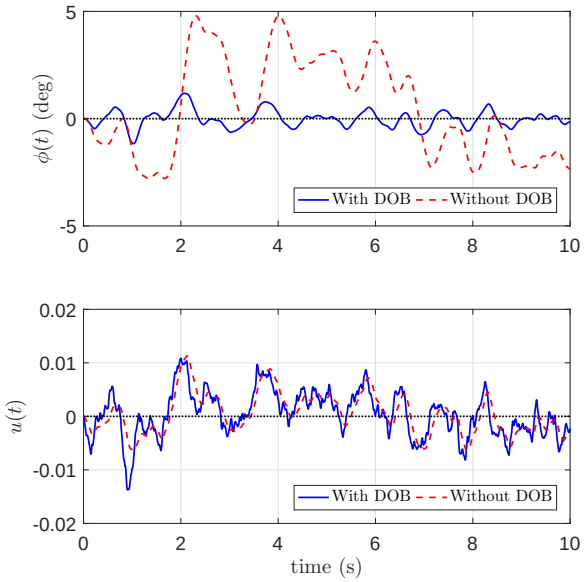

Figure 7: Effect of the uncertainty estimator in disturbance rejection

Finally, a third simulation is included to illustrate the capabilities of the proposed controller when rejecting external time-varying disturbances. To this purpose, some turbulent wind is simulated by passing white noise through a low-pass filter and, then, it is input to the system. Figure 7, and Table 3, show a comparison of the proposed control strategy and an scenario in which the uncertainty is not compensated, that is, setting $\hat{\boldsymbol{\sigma}} = 0$.

6. Experiments

A quadrotor prototype composed of an F330 DJI frame, DJI motors 2212 920 Kv, Hobbywing ESCs 20 A, 8045 self-tightening propellers and a battery ACE 4000 mAh 3s 11.1 V 25C LIPO is used for the experiments (see Fig. 8). The computational power is provided by a Pixhawk running PX4 firmware 1.4.2 in which the proposed control algorithm has been programed. The control parameters and

Figure 8: Quadrotor prototype.

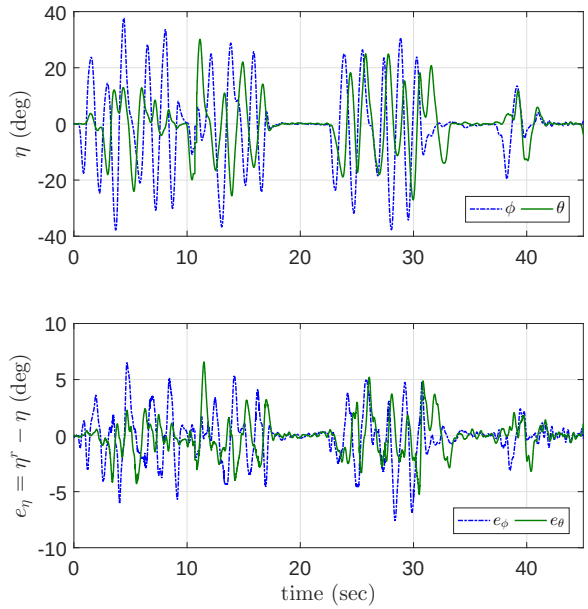

Figure 9: Experimental data recorded during a remotely piloted flight.

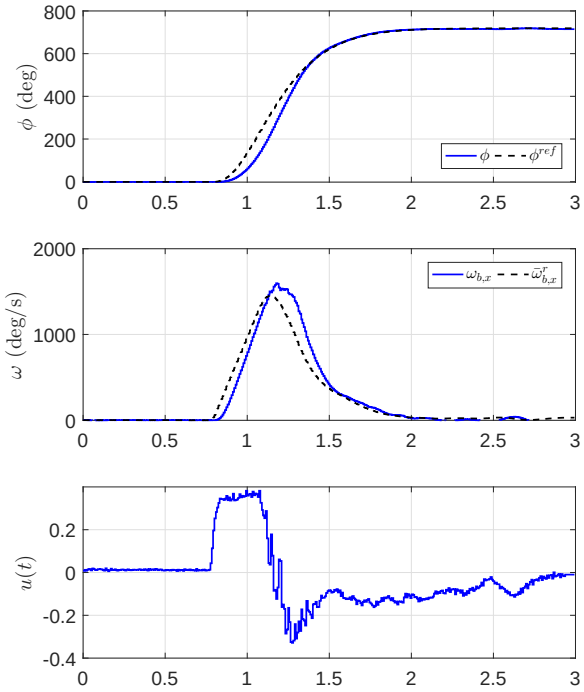

Figure 10: Experimental data recorded during a double-loop maneuver. A video of this experiment can be seen in `https://youtu.be/lBR78sg2T_E`

the identified parameters are the same as the ones used in simulations. Several flights have been performed in order to validate the different features of the proposed controller.

Overall performance: Two experiments are carried out to simply evaluate the tracking performance. First, a remotely piloted flight is performed indoors and aggressive roll and pitch references are given through a remote controller. The results of this experiment can be seen in Fig. 9. The upper plot shows the quadrotor's roll, ϕ, and pitch, θ, angles; while the lower plot depicts the trajectory tracking errors. The analysis of the data reveals a Root Mean Square Error (RMSE) of 2.0 deg and 1.57 deg for the roll and pitch angles, respectively. This is a fairly good performance taking into account that the angular references reach ± 40 deg and ± 30 deg in roll and pitch axes, respectively.

A second experiment is performed outdoors in which a double-loop attitude trajectory is commanded to the quadrotor. This experiment is performed in order to test the tracking performance when high aggressive maneuvers are being performed. The data recorded during this experiment is shown in Fig. 10, where it can be seen a fairly good reference tracking even under this circumstances of very high angular velocities/accelerations. It is needed to remark that, for safety, the angular acceleration, $\ddot{\bar{\omega}}^r_b$, has been limited in this experiment. This is performed by a small change in the TD (12), i.e. it is replaced by the one presented in Castillo et al. (2016), which maintains the same stability properties. A video of this experiment can be seen in `https://youtu.be/lBR78sg2T_E`.

Tracking performance: In order to validate the controller trajectory tracking performance, the same scenario as in the second simulation of Section 5 is reproduced in this experiment. The quadrotor response, which is depicted in Fig. 11, reveals almost the same response as in the simulation of Fig. 5. The analysis of the data reveal a RMSE of 0.97, 0.96 and 0.66 deg for the roll, pitch and yaw axis, respectively.

Disturbance rejection: The disturbance observer plays an important role in the performance of the controller as it has been shown through different simulations in Section 5. For a better illustration, two experiments are reported here. The first one is performed only in the roll axis. A sinusoidal input signal is artificially added to the generated control action just before it is sent to the motors while the quadrotor is at hover. In this sense, the disturbance observer should detect this signal as an unknown external disturbance, and it should generate the required control action in order to cancel its effect, i.e. the same signal. This experiment is performed twice, with and without disturbance compensation. One can see in Fig. 12 that the disturbance observer is able to reproduce the same disturbance signal, mitigating substantially the deviation in the roll angle. This experiment also points out the performance improvement at hover (during the first 4 s), as the deviation of the roll angle from zero drops from ± 2 deg to ± 0.2 deg when the compensation is active. Note also that before, and after, the disturbance is introduced, the DOB is also observing other disturbances (because $\hat{\sigma} \neq 0$); this is probably caused by minor external disturbances affecting to the quadrotor during the experiment.

Finally, the second experiment is intended to demonstrate the usefulness of the proposed control strategy. A

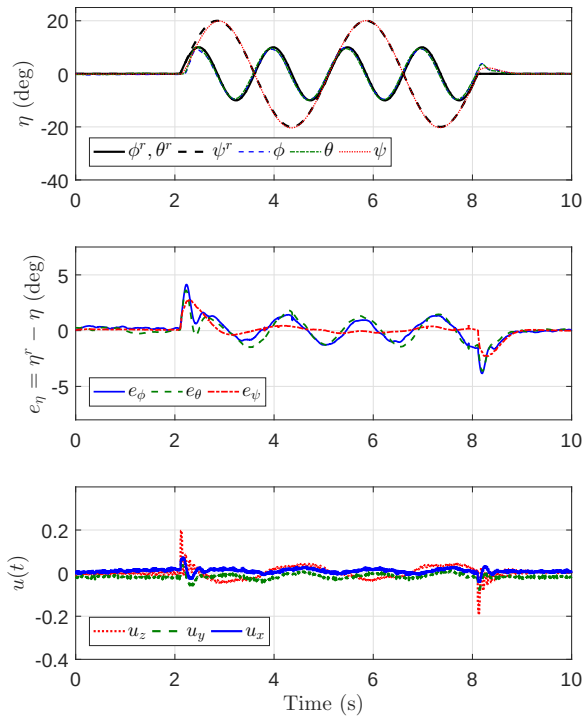

Figure 11: Experimental results showing tracking of sinusoidal references.

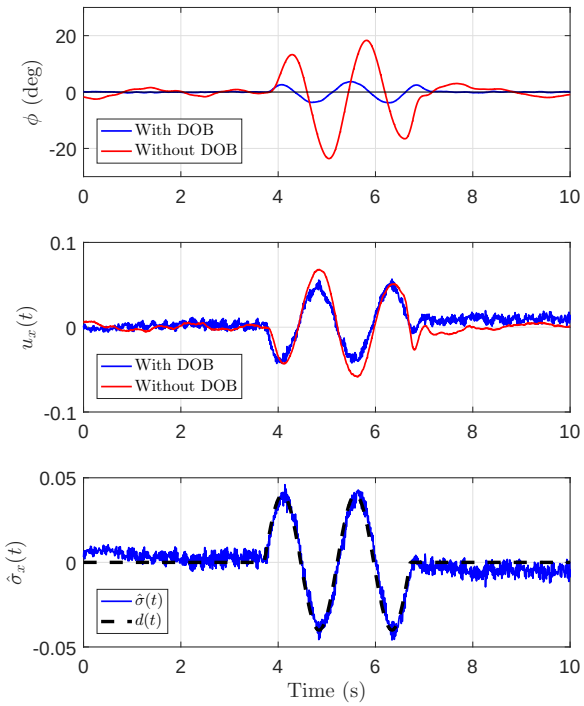

Figure 12: Experimental comparison showing the effect of the observer compensation when an input sinusoidal disturbance is applied.

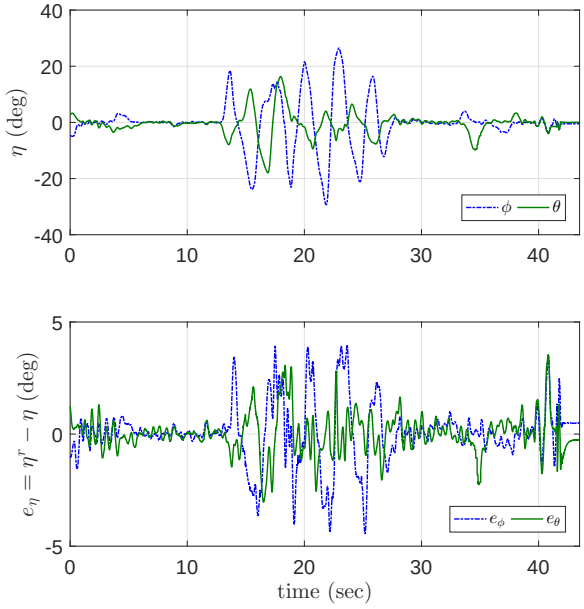

Figure 13: Experimental results showing the tracking of references with a suspended payload. A video of this experiment can seen in `https://youtu.be/-QZgOm_jtIo`

suspended load of about 100 g, which can be regarded as an external disturbance, is attached at the end of one of the quadrotor arms. A remotely piloted flight is carried out in this scenario. The results can also be seen in Figure 13. Also, a video of this experiment can seen in `https://youtu.be/-QZgOm_jtIo`. The analysis of the recorded data reveals a RMSE of about 1.2 deg and 0.9 deg in the roll and pitch angles, respectively, which is remarkable.

7. Conclusions

In this paper, a new disturbance observer-based quadrotor attitude control has been proposed. The conventional hypothesis of small angles, knowledge of the inertia matrix, absence of external disturbances and fast motor dynamics are avoided in the controller design. This permits to the resulting controller to perform precise and aggressive attitude maneuvers in disturbed environments. The controller is relatively simple to implement and only two quadrotor parameters need to be identified. The stability of the whole closed-loop system has been analyzed in terms of Lyapunov's theory. Simulations and experiments show an outstanding control performance of the proposed controller, even in the presence of important time-varying external disturbances.

Acknowledgment

This work was partially supported by projects FPU15/02008, FPI-UPV 2014 and TIN2014-56158-C4-4-P-AR, Ministerio de Economia y Competitividad, Spain.

The authors would like to thank Prof. Pedro Albertos for his valuable comments on the technical content of the paper. The authors would also like to acknowledge the Associate Editor and anonymous reviewers for their insightful comments, which considerably improved the quality of this paper.

Appendix A. Proof of Theorem 1

Consider the Lyapunov candidate function $V = \boldsymbol{x}^T \boldsymbol{P} \boldsymbol{x}$, whose time-derivative along the trajectories of (22) is given by

$$\dot{V} = \boldsymbol{x}^T (\boldsymbol{P}\boldsymbol{A} + \boldsymbol{A}^T \boldsymbol{P})\boldsymbol{x} + 2\boldsymbol{x}^T \boldsymbol{P}_2 \dot{\boldsymbol{\sigma}} - 2\boldsymbol{x}^T \boldsymbol{P}_3 \boldsymbol{B}^{-1} \ddot{\boldsymbol{\omega}}_{\boldsymbol{b}}^{\boldsymbol{r}},$$

which, for all $\|\boldsymbol{x}\| \leq \beta_{\sigma_3}$, it is norm-bounded by

$$\|\dot{V}\| \leq \Big[\big(-\underline{\lambda}(\boldsymbol{P}\boldsymbol{A} + \boldsymbol{A}^T \boldsymbol{P}) + 2\|\boldsymbol{P}_2\|\beta_{\sigma_1} \big)\|\boldsymbol{x}\| + \\ + \big(2\big\|\boldsymbol{P}_3 \boldsymbol{B}^{-1}\big\|\beta_{\ddot{\bar{\omega}}_b^r} + 2\|\boldsymbol{P}_2\|\beta_{\sigma_2} \big) \Big] \|\boldsymbol{x}\|.$$

Then, for a small β_{σ_1}, i.e. $\beta_{\sigma_1} < \frac{\underline{\lambda}\left(\boldsymbol{P}\boldsymbol{A} + \boldsymbol{A}^T \boldsymbol{P}\right)}{2\|\boldsymbol{P}_2\|}$, it is verified that $\big(-\underline{\lambda}(\boldsymbol{P}\boldsymbol{A} + \boldsymbol{A}^T \boldsymbol{P}) + 2\|\boldsymbol{P}_2\|\beta_{\sigma_1} \big) < 0$; and, therefore, $\dot{V} < 0$ for all $\boldsymbol{x}$ such that,

$$\beta_{\sigma_3} \geq \|\boldsymbol{x}\| > \frac{2\big\|\boldsymbol{P}_3 \boldsymbol{B}^{-1}\big\|\beta_{\ddot{\bar{\omega}}_b^r} + 2\|\boldsymbol{P}_2\|\beta_{\sigma_2}}{\underline{\lambda}(\boldsymbol{P}\boldsymbol{A} + \boldsymbol{A}^T \boldsymbol{P}) - 2\|\boldsymbol{P}_2\|\beta_{\sigma_1}} \triangleq x^*.$$

This leads to the bound-condition over β_{σ_1}, β_{σ_3} and it also implies that, if $\|\boldsymbol{x}(0)\| \leq x^*$, then $\|\boldsymbol{x}(t)\| \leq x^*$ for all t.

Appendix B. Proof of Proposition 2

First, let us prove the existence of $\beta_{\ddot{\bar{\omega}}_b^r}$ such that $\|\ddot{\boldsymbol{\omega}}_{\boldsymbol{b}}^{\boldsymbol{r}}\| \leq \beta_{\ddot{\bar{\omega}}_b^r}$. Under Assumption 2, the reference angular velocity generated by (11) is bounded by

$$\|\boldsymbol{\omega}_{\boldsymbol{b}}^{\boldsymbol{r}}\| = \|\boldsymbol{R}^T(q_e)\boldsymbol{\omega}_{\boldsymbol{d}}(t) - k\boldsymbol{q}_{\boldsymbol{e}}\| \leq \|\boldsymbol{\omega}_{\boldsymbol{d}}(t)\| + k\|\boldsymbol{q}_{\boldsymbol{e}}\|, \\ \leq \beta_{\omega_d} + k. \tag{B.1}$$

Therefore, as $\boldsymbol{\omega}_b^r$ is bounded and due to the internal stable dynamics of the TD (12), the variables $\bar{\boldsymbol{\omega}}_{\boldsymbol{b}}^{\boldsymbol{r}}$, $\dot{\bar{\boldsymbol{\omega}}}_{\boldsymbol{b}}^{\boldsymbol{r}}$, $\ddot{\bar{\boldsymbol{\omega}}}_{\boldsymbol{b}}^{\boldsymbol{r}}$ in (12) are also bounded. This proves the existence constants $\beta_{\bar{\omega}_b^r}$, $\beta_{\dot{\bar{\omega}}_b^r}$, $\beta_{\ddot{\bar{\omega}}_b^r} \geq 0$ such that

$$\|\bar{\boldsymbol{\omega}}_{\boldsymbol{b}}^{\boldsymbol{r}}\| \leq \beta_{\bar{\omega}_b^r}, \quad \|\dot{\bar{\boldsymbol{\omega}}}_{\boldsymbol{b}}^{\boldsymbol{r}}\| \leq \beta_{\dot{\bar{\omega}}_b^r}, \quad \|\ddot{\bar{\boldsymbol{\omega}}}_{\boldsymbol{b}}^{\boldsymbol{r}}\| \leq \beta_{\ddot{\bar{\omega}}_b^r}, \tag{B.2}$$

which proves the first statement.

Now, let us prove the existence of $\beta_{\sigma_1}, \beta_{\sigma_2}, \beta_{\sigma_3}$ such that $\|\dot{\boldsymbol{\sigma}}\| \leq \beta_{\sigma_1}\|\boldsymbol{x}\| + \beta_{\sigma_2}, \forall \|\boldsymbol{x}\| \leq \beta_{\sigma_3}$. Recalling that $\boldsymbol{\sigma}(\boldsymbol{w_b}, t) = \boldsymbol{K_u}^{-1}\boldsymbol{\tau_\delta}(t) - \boldsymbol{K_u}^{-1}\boldsymbol{S}(\boldsymbol{\omega_b})\boldsymbol{J}\boldsymbol{\omega_b}$, then

$$\dot{\boldsymbol{\sigma}} = \boldsymbol{K_u}^{-1}\left(\dot{\boldsymbol{\tau}}_{\boldsymbol{\delta}}(t) - \frac{d}{dt}\big(\boldsymbol{S}(\boldsymbol{\omega_b})\boldsymbol{J}\boldsymbol{\omega_b}\big) \right)$$

where the second element constitutes the time-derivative of the Coriolis term. It is not hard to verify that

$$\frac{d}{dt}\big(\boldsymbol{S}(\boldsymbol{\omega_b})\boldsymbol{J}\boldsymbol{\omega_b}\big) = \big(\boldsymbol{S}(\boldsymbol{\omega_b})\boldsymbol{J} - \boldsymbol{S}(\boldsymbol{J}\boldsymbol{\omega_b})\big)\dot{\boldsymbol{\omega}}_{\boldsymbol{b}}$$

and therefore

$$\|\dot{\boldsymbol{\sigma}}\| \leq \|\boldsymbol{K_u}^{-1}\| \left(\|\dot{\boldsymbol{\tau}}_{\boldsymbol{\delta}}(t)\| + \Big\|\big(\boldsymbol{S}(\boldsymbol{\omega_b})\boldsymbol{J} - \boldsymbol{S}(\boldsymbol{J}\boldsymbol{\omega_b})\big)\Big\|\|\dot{\boldsymbol{\omega}}_{\boldsymbol{b}}\| \right) \\ \leq \|\boldsymbol{K_u}^{-1}\| \Big(\|\dot{\boldsymbol{\tau}}_{\boldsymbol{\delta}}(t)\| + 2\big\|\boldsymbol{J}\big\|\|\boldsymbol{\omega_b}\|\|\dot{\boldsymbol{\omega}}_{\boldsymbol{b}}\| \Big). \tag{B.3}$$

Then, by the definition of the angular velocity tracking error, $\boldsymbol{z} \triangleq \boldsymbol{\omega_b} - \bar{\boldsymbol{\omega}}_{\boldsymbol{b}}^{\boldsymbol{r}}$, see Figure 2; by (B.2), by (22); and by the fact that $\|\boldsymbol{z}\| \leq \|\boldsymbol{x}\|$; it is verified that

$$\|\boldsymbol{\omega_b}\| = \|\boldsymbol{z} + \bar{\boldsymbol{\omega}}_{\boldsymbol{b}}^{\boldsymbol{r}}\| \leq \|\boldsymbol{x}\| + \beta_{\bar{\omega}_b^r} \tag{B.4}$$

$$\|\dot{\boldsymbol{\omega}}_{\boldsymbol{b}}\| = \|\dot{\boldsymbol{z}} + \dot{\bar{\boldsymbol{\omega}}}_{\boldsymbol{b}}^{\boldsymbol{r}}\| = \big\|[-\boldsymbol{K},\, \boldsymbol{B},\, \boldsymbol{B}]\boldsymbol{x} + \dot{\bar{\boldsymbol{\omega}}}_{\boldsymbol{b}}^{\boldsymbol{r}}\big\| \\ \leq \beta_z\|\boldsymbol{x}\| + \beta_{\dot{\bar{\omega}}_b^r}, \tag{B.5}$$

where $\beta_z = \big\|[-\boldsymbol{K},\, \boldsymbol{B},\, \boldsymbol{B}]\big\|$. Substituting (B.4)-(B.5) into (B.3) and incorporating Assumption 1 it is obtained that

$$\|\dot{\boldsymbol{\sigma}}\| \leq 2\beta_z\big\|\boldsymbol{K_u}^{-1}\big\|\big\|\boldsymbol{J}\big\|\|\boldsymbol{x}\|^2 + \\ + 2\big\|\boldsymbol{K_u}^{-1}\big\|\big\|\boldsymbol{J}\big\|\big(\beta_{\omega_d} + \beta_{\dot{\bar{\omega}}_b^r}\big)\|\boldsymbol{x}\| + \\ + \big\|\boldsymbol{K_u}^{-1}\big\|\beta_{\tau_\delta} + 2\beta_{\bar{\omega}_d}\beta_{\bar{\omega}_b^r}\big\|\boldsymbol{K_u}^{-1}\big\|.$$

and, therefore, as $\|\dot{\boldsymbol{\sigma}}\| \leq \alpha_1\|\boldsymbol{x}\|^2 + \alpha_2\|\boldsymbol{x}\| + \alpha_3$ with $\alpha_1, \alpha_2, \alpha_3 \geq 0$, then, one can find constants β_{σ_1}, β_{σ_2}, β_{σ_3}, such that $\|\dot{\boldsymbol{\sigma}}\| \leq \beta_{\sigma_1}\|\boldsymbol{x}\| + \beta_{\sigma_2}$, $\forall \|\boldsymbol{x}\| \leq \beta_{\sigma_3}$.

Appendix C. Proof of Theorem 2

First, let us obtain an expression for the time-derivative of the attitude error, $\dot{q}_e$. Differentiating (10) and incorporating (3) and (9) it is obtained that the attitude error obeys the following differential equation (refer to (Tayebi, 2008) for details)

$$\begin{cases} \dot{q}_{e_0} = -\dfrac{1}{2}\boldsymbol{q_e}^T\big(\boldsymbol{\omega_b} - \boldsymbol{R}^T(q_e)\boldsymbol{\omega_d}(t)\big), \\ \dot{\boldsymbol{q}}_{\boldsymbol{e}} = \dfrac{1}{2}\left[q_{e_0}\boldsymbol{I_3} + \boldsymbol{S}(\boldsymbol{q_e})\right]\big(\boldsymbol{\omega_b} - \boldsymbol{R}^T(q_e)\boldsymbol{\omega_d}(t)\big). \end{cases} \tag{C.1}$$

where $\boldsymbol{R}(q_e)$ is given by (2).

Now, let us express (C.1) in terms of $\boldsymbol{z}$ and in terms of the angular velocity reference signal error, $\tilde{\boldsymbol{\omega}}_{\boldsymbol{b}}^{\boldsymbol{r}}$, introduced by the TD, which is defined as:

$$\tilde{\boldsymbol{\omega}}_{\boldsymbol{b}}^{\boldsymbol{r}} \triangleq \boldsymbol{\omega}_b^r - \bar{\boldsymbol{\omega}}_{\boldsymbol{b}}^{\boldsymbol{r}}. \tag{C.2}$$

Recalling that $\boldsymbol{\omega_b} = \boldsymbol{z} + \bar{\boldsymbol{\omega}}_{\boldsymbol{b}}^{\boldsymbol{r}} = \boldsymbol{z} + \boldsymbol{\omega}_b^r - \tilde{\boldsymbol{\omega}}_{\boldsymbol{b}}^{\boldsymbol{r}}$, incorporating (11) and substituting the resulting expression into (C.1) leads to

$$\begin{cases} \dot{q}_{e_0} = -\dfrac{1}{2}\boldsymbol{q_e}^T\big(\boldsymbol{z} - \tilde{\boldsymbol{\omega}}_{\boldsymbol{b}}^{\boldsymbol{r}} - k\boldsymbol{q_e}\big), \\ \dot{\boldsymbol{q}}_{\boldsymbol{e}} = \dfrac{1}{2}\left[q_{e_0}\boldsymbol{I_3} + \boldsymbol{S}(\boldsymbol{q_e})\right]\big(\boldsymbol{z} - \tilde{\boldsymbol{\omega}}_{\boldsymbol{b}}^{\boldsymbol{r}} - k\boldsymbol{q_e}\big). \end{cases} \tag{C.3}$$

Let us now consider the Lyapunov candidate function

$$V = (1 - q_{e_0})^2 + \boldsymbol{q_e}^T\boldsymbol{q_e} = 2(1 - q_{e_0}), \tag{C.4}$$

whose time-derivative along the trajectories of (C.3) is

$$\begin{aligned}\dot{V} &= -k\|\boldsymbol{q_e}\|^2 + \boldsymbol{q_e}^T(\boldsymbol{z} - \tilde{\boldsymbol{\omega}}_{\boldsymbol{b}}^{\boldsymbol{r}}) \\ &\leq \|\boldsymbol{q_e}\|\Big(-k\|\boldsymbol{q_e}\| + \|\boldsymbol{z}(t)\| + \|\tilde{\boldsymbol{\omega}}_{\boldsymbol{b}}^{\boldsymbol{r}}\|\Big) \\ &\leq \|\boldsymbol{q_e}\|\Big(-k\|\boldsymbol{q_e}\| + \epsilon_z + \epsilon_\omega\Big) = \\ &= \sqrt{1-q_{e_0}^2}\Big(-k\sqrt{1-q_{e_0}^2} + \epsilon_z + \epsilon_\omega\Big),\end{aligned} \tag{C.5}$$

where $\epsilon_z, \epsilon_\omega \geq 0$ are the upper bounds of $\|\boldsymbol{z}(t)\|$ and $\|\tilde{\boldsymbol{\omega}}_{\boldsymbol{b}}^{\boldsymbol{r}}(t)\|$, respectively.

Therefore, if $k > \epsilon_z + \epsilon_\omega$ then, by (C.5), it holds that $\dot{V} < 0$, for all

$$-\sqrt{1-\left(\frac{\epsilon_z+\epsilon_\omega}{k}\right)^2} < q_{e_0} < \sqrt{1-\left(\frac{\epsilon_z+\epsilon_\omega}{k}\right)^2},$$

which implies that, if $q_{e_0}(0) > \sqrt{1-\left(\frac{\epsilon_z+\epsilon_\omega}{k}\right)^2}$, then the attitude error is bounded by (23) for all t.

Bibliography

Altug, E., Ostrowski, J. P., Mahony, R., 2002. Control of a quadrotor helicopter using visual feedback. In: Robotics and Automation 2002. Proceedings. ICRA'02. IEEE International Conference on. Vol. 1. IEEE, pp. 72–77.

Bhat, S. P., Bernstein, D. S., 2000. A topological obstruction to continuous global stabilization of rotational motion and the unwinding phenomenon. Systems & Control Letters 39 (1), 63–70.

Bouabdallah, S., Noth, A., Siegwart, R., 2004. PID vs LQ control techniques applied to an indoor micro quadrotor. In: Intelligent Robots and Systems, 2004. Proceedings. IROS'04. IEEE/RSJ International Conference on. Vol. 3. IEEE, pp. 2451–2456.

Bouabdallah, S., Siegwart, R., 2007. Full control of a quadrotor. In: Intelligent Robots and Systems, 2007. Proceedings. IROS'07. IEEE/RSJ International Conference on. IEEE, pp. 153–158.

Castillo, A., García, P., Sanz, R., Albertos, P., 2018. Enhanced extended state observer-based control for systems with mismatched uncertainties and disturbances. ISA transactions 73, 1–10.

Castillo, A., Sanz, R., Garcia, P., Albertos, P., 2016. A quaternion-based and active disturbance rejection attitude control for quadrotor. In: Information and Automation, 2016. ICIA. IEEE International Conference on. IEEE.

Castillo, P., Dzul, A., Lozano, R., 2003. Real-time stabilization and tracking of a four rotor mini-rotorcraft. In: European Control Conference, 2003. Proceedings. ECC. IEEE, pp. 3123–3128.

Castillo, P., Lozano, R., Dzul, A. E., 2005. Modelling and control of mini-flying machines. Physica-Verlag.

Chen, W. H., Yang, J., Guo, L., Li, S., 2016. Disturbance-observer-based control and related methods—An overview. IEEE Transactions on Industrial Electronics 63 (2), 1083–1095.

Chen, Z., Huang, J., 2009. Attitude tracking and disturbance rejection of rigid spacecraft by adaptive control. IEEE Transactions on Automatic Control 54 (3), 600–605.

Chovancová, A., Fico, T., Chovanec, L., Hubinsk, P., 2014. Mathematical modelling and parameter identification of quadrotor (a survey). Procedia Engineering 96, 172–181.

Derafa, L., Madani, T., Benallegue, A., 2006. Dynamic modelling and experimental identification of four rotors helicopter parameters. In: Industrial Technology, 2006. ICIT 2006. IEEE International Conference on. IEEE, pp. 1834–1839.

Erginer, B., Altug, E., 2007. Modeling and PD control of a quadrotor VTOL vehicle. In: Intelligent Vehicles Symposium, 2007. Proceedings. IV'07. IEEE, pp. 894–899.

Fresk, E., Nikolakopoulos, G., 2013. Full quaternion based attitude control for a quadrotor. In: European Control Conference, 2013. Proceedings. ECC. pp. 17–19.

Guerrero-Castellanos, J., Marchand, N., Hably, A., Lesecq, S., Delamare, J., 2011. Bounded attitude control of rigid bodies: Real-time experimentation to a quadrotor mini-helicopter. Control Engineering Practice 19 (8), 790–797.

Hahn, W., 1967. Stability of motion. Vol. 138. Springer.

Hoffmann, G., Rajnarayan, D. G., Waslander, S. L., Dostal, D., Jang, J. S., Tomlin, C. J., 2004. The Stanford testbed of autonomous rotorcraft for multi agent control (STARMAC). In: Digital Avionics Systems Conference, 2004. Proceedings. DASC 04. The 23rd. Vol. 2. IEEE, pp. 12–E.

Hoffmann, G. M., Huang, H., Waslander, S. L., Tomlin, C. J., 2007. Quadrotor helicopter flight dynamics and control: Theory and experiment. In: Guidance, Navigation, and Control Conference, 2007. Proceedings. AIAA. Vol. 2. p. 4.

Jia, Y.-B., 2013. Quaternions and rotations. Com S 477 (577), 15.

Kuipers, J. B., et al., 1999. Quaternions and rotation sequences. Vol. 66. Princeton University Press Princeton.

Lee, T., 2012. Exponential stability of an attitude tracking control system on SO(3) for large-angle rotational maneuvers. Systems & Control Letters 61 (1), 231–237.

Lee, T., Leok, M., McClamroch, N. H., 2013. Nonlinear robust tracking control of a quadrotor UAV on SE(3). Asian Journal of Control 15 (2), 391–408.

Liu, H., Wang, X., 2015. Quaternion-based robust attitude control for quadrotors. In: Unmanned Aircraft Systems, 2015. ICUAS. International Conference on. IEEE, pp. 920–925.

Liu, H., Zhao, W., Zuo, Z., Zhong, Y., 2017. Robust control for quadrotors with multiple time-varying uncertainties and delays. IEEE Transactions on Industrial Electronics 64 (2), 1303–1312.

Madani, T., Benallegue, A., 2006. Control of a quadrotor mini-helicopter via full state backstepping technique. In: Decision and Control, 2006. Proceedings. 45th IEEE Conference on. IEEE, pp. 1515–1520.

Mayhew, C. G., Sanfelice, R. G., Teel, A. R., 2011. Quaternion-based hybrid control for robust global attitude tracking. IEEE Transactions on Automatic Control 56 (11), 2555–2566.

Mazinan, A., Pasand, M., Soltani, B., 2015. Full quaternion based finite-time cascade attitude control approach via pulse modulation synthesis for a spacecraft. ISA transactions 58, 567–585.

Michael, N., Mellinger, D., Lindsey, Q., Kumar, V., 2010. The grasp multiple micro-UAV testbed. IEEE Robotics & Automation Magazine 17 (3), 56–65.

Pounds, P., Mahony, R., Corke, P., 2010. Modelling and control of a large quadrotor robot. Control Engineering Practice 18 (7), 691–699.

Raffo, G. V., Ortega, M. G., Rubio, F. R., 2010. An integral predictive/nonlinear H_∞ control structure for a quadrotor helicopter. Automatica 46 (1), 29–39.

Sanz, R., Garcia, P., Zhong, Q.-C., Albertos, P., 2016. Robust control of quadrotors based on an uncertainty and disturbance estimator. Journal of Dynamic Systems, Measurement, and Control 138 (7).

Schlanbusch, R., Loria, A., Nicklasson, P. J., 2012. On the stability and stabilization of quaternion equilibria of rigid bodies. Automatica 48 (12), 3135–3141.

Shuster, M. D., 1993. A survey of attitude representations. Navigation 8 (9), 439–517.

Tayebi, A., 2008. Unit quaternion-based output feedback for the attitude tracking problem. IEEE Transactions on Automatic Control 53 (6), 1516–1520.

Tayebi, A., McGilvray, S., 2006. Attitude stabilization of a VTOL quadrotor aircraft. IEEE Transactions on Control Systems Technology 14 (3), 562–571.

Wang, L., Su, J., 2015. Robust disturbance rejection control for attitude tracking of an aircraft. IEEE Transactions on Control Systems Technology 23 (6), 2361–2368.

Wang, X., Shirinzadeh, B., Ang, M. H., 2015. Nonlinear double-integral observer and application to quadrotor aircraft. IEEE Transactions on Industrial Electronics 62 (2), 1189–1200.

Xiao, B., Yin, S., 2017. A new disturbance attenuation control scheme for quadrotor unmanned aerial vehicles. IEEE Transactions on Industrial Informatics 13 (6), 2922–2932.

Zhang, R., Quan, Q., Cai, K.-Y., 2011. Attitude control of a quadrotor aircraft subject to a class of time-varying disturbances. IET Control Theory & Applications 5 (9), 1140–1146.

Zhang, Y., Wang, L., 2015. Anti-disturbance control methodology for attitude tracking of an UAV. In: Robotics and Biomimetics, 2015. ROBIO. IEEE International Conference on. IEEE, pp. 837–842.